THE ASTROPHYSICAL JOURNAL, 428:447–453, 1994 June 20

ARCMINUTE SKY FLUCTUATIONS AT 1.25 MILLIMETERS[1]

PAOLA ANDREANI
Dipartimento di Astronomia, Università di Padova, vicolo dell'Osservatorio 5, 35122 Padova, Italy;
e-mail: andreani@astrpd.astro.it
Received 1993 July 19; accepted 1993 December 17

ABSTRACT

Observations of radio-quiet quasars made by the Swedish ESO Submillimeter Telescope and the Institut de Radio Astronomie Millimetrique antenna at a frequency of 240 GHz have been used to infer upper limits on the sky fluctuations at angular scales of 30″, 70″, and 140″. It is found that $\Delta T/T < 1.4 \times 10^{-4}$ at 30″, $\Delta T/T < 2.4 \times 10^{-4}$ at 70″, and $\Delta T/T < 1.9 \times 10^{-4}$ at 140″ (95% confidence level) for uncorrelated patches of sky. The two former limits are 70% and 10% higher, respectively, if detections of radio-quiet objects are included in the analysis. These limits can be used in the context of (1) models predicting far-infrared cosmic backgrounds originating from primeval dust and (2) models of dusty galaxy evolution. On the basis of these data, most of the primeval dust models can be ruled out and further constraints on the galaxy population contributing to the background can be determined.

Subject headings: cosmic background radiation — cosmology: observations — diffuse radiation — infrared: general

1. INTRODUCTION

A fundamental key to probing the "dark ages" of the universe between the epoch of galaxy formation and that of decoupling at much higher redshifts ($z \sim 1000$) would be the detection of an infrared/submillimeter background. Such a background is expected to arise either from the integrated emission of unresolved protostructures, such as primeval galaxies, Population III stars, and other sources of pregalactic origin (halo very massive objects [VMOs], black holes in galactic nuclei and in the galactic halos, and pregalactic explosions), and/or thermal emission produced by associated and coeval dust. The energy domain in which to look for radiation originating in the redshift range 5–1000 is very likely the far-infrared (100–1000 μm), where dust reradiation is expected to appear and where the universe is optically thin.

The existence of cosmological backgrounds distinct from the cosmic background radiation (CBR) has been widely discussed in the past: earlier works (Partridge & Peebles 1967; Tinsley 1973) concentrate on the near-infrared, while later works put more emphasis on the far-infrared components (Stecker, Puget, & Fazio 1977; Rowan-Robinson, Negroponte, & Silk 1979; Bond, Carr & Hogan 1986, 1991 [hereafter BCH91]; Negroponte 1986). The detection of these backgrounds is a very difficult task because of the presence of the intense *local* backgrounds: the atmosphere and the interplanetary and interstellar dust. The CBR itself hides any other background above 400 μm.

Limits on the energy density of a cosmological background different from the CBR in the wavelength range $5000 > \lambda > 500$ μm have been fixed by the *COBE*-FIRAS data. From the upper limit on the deviations from a pure blackbody spectrum of the CBR, 0.03% in brightness, it turns out that any other cosmological background with spectrum different from that of the Galaxy in this wavelength range should have an energy density $\Omega_{R,FIR} h^2 \leqslant 10^{-7}$ (i.e., $\nu I_\nu < 4.1 \times 10^{-13}$ W cm^{-2} sr^{-1}) (Wright et al. 1993).

To avoid the difficult task of performing absolute measurements, we use the easier approach of studying the angular radiation distribution. Cosmological sources producing these backgrounds would leave a recognizable imprint on the angular radiation pattern (BCH91, and references therein). However, a fundamental limit is represented by the brightness fluctuations originating from dusty galaxies at redshift $z \leq 0.5$. Galaxies may represent the dominant component of infrared/submillimeter backgrounds and surely contribute significantly to the *confusion limit*, hampering any cosmological signature at these wavelengths (e.g., Franceschini et al. 1989, 1991; Saunders et al. 1990; Oliver, Rowan-Robinson, & Saunders 1992).

In this paper, ground-based observations collected by the Institut de Radio Astronomie Millimetrique antenna (IRAM) and the Swedish ESO Submillimeter Telescope (SEST) of high-redshift radio-quiet quasars (§ 2) and the data analysis procedure (§ 3) are described in detail. The upper limits to the sky fluctuations at three different angular scales: 30″, 70″, and 140″ are estimated (§ 4), and the implications are discussed within the framework of (1) secondary anisotropies of the microwave sky and (2) the source confusion limit (§ 5).

2. THE OBSERVATIONS

The observations were carried out during 1990 May and 1991 March with the IRAM 30 m antenna located at Pico Veleta (Spain) and during 1991 September and 1992 September with the SEST 15 m telescope in Chile. Both telescopes fed a ^{3}He-cooled bolometer (Kreysa 1990). The filter set coupled to the atmospheric transmission window provides an effective wavelength around 1.25 mm. The beam sizes, ϕ_{FWHM}, of the two instruments are 11″ and 24″, respectively. The IRAM system had an average sensitivity, mainly due to atmospheric noise, of 60 mJy Hz$^{-1/2}$. During the last SEST run, because of extraordinary atmospheric stability, we were most of the time constrained only by detector noise (140 mJy Hz$^{-1/2}$), while during the first run the average sensitivity was 200 mJy Hz$^{-1/2}$, because of weather conditions.

In order to minimize spurious signals, such as ground pickup and atmospheric effects, observations were always per-

[1] Based on observations at the SEST 15 m telescope (Chile) and at the IRAM 30 m antenna (Spain).

formed at elevation angles greater than 60°, starting before culmination and ending after culmination of each source. Each object was observed more than 3 times, in different days, for $200n$ s, with n ranging between 8 and 10, with the standard ON-ON technique; i.e., the sky emission in the direction of the source (I_S) has been compared with that of two empty sky regions (I_A and I_B) located beside the source at constant elevation by means of either a chopper wheel or a wobbling secondary. The resulting signal for each ON-ON is

$$\Delta I = I_S - \frac{(I_A + I_B)}{2}, \tag{1}$$

where I is the sky intensity in mJy. This double-switching technique combined with azimuth chopping successfully eliminates any position-dependent offsets and the constant and linear atmospheric trends, but higher order terms survive (see also Church, Lasenby, & Hills 1993).

Atmospheric transmission was monitored by frequent skydips; i.e., telescope scans at constant azimuth and different elevation were carried out to compare the atmospheric emission with that of an absorber moved into the path of the reference beam. Beam switching is achieved at IRAM by wobbling the secondary in azimuth. At SEST, spatial modulation is obtained with a chopper wheel located in the receiver cabin. The wobbling amplitude for IRAM and the chop throw for SEST were $\phi_s = 30''$ and $\phi_s = 70''$, respectively. Uranus, Mars, Neptune, and Saturn have been used as primary calibrators, and several radio-loud quasars as secondary calibrators, mainly to detect sky variations during the observations. The final absolute calibration is accurate to within 10%.

The millimeter flux values have been corrected for the overall system response, evaluated by computing the integral

$$\Re(w, \alpha, El) = \int_{\nu_1}^{\nu_2} I_{\rm atm}(\nu, w, El)\Upsilon(\nu)\epsilon(\nu, El)\left(\frac{\nu}{\nu_0}\right)^{\alpha} d\nu,$$

where ν_1 and ν_2 are the lower and upper limits of the system spectral response, El is the elevation of the source, $\epsilon(\nu, El)$ is the antenna efficiency, $\Upsilon(\nu)$ is the transmission curve of the optics, α is the spectral index of the sources (which are assumed to have a spectrum in the millimetric region approximated by $F = F_0(\nu/\nu_0)^{\alpha}$), and $I_{\rm atm}(\nu, w)$ is the spectral dependence of the atmospheric emission and absorption (Liebe 1983), assumed to follow a cosecant law: $I(\nu, w) \propto I(\nu)e^{-\tau_0(w)\csc El}$, $\tau_0(w)$ being the measured zenith optical depth for a given value of water vapor content w. Some of the observed sources have been detected: data and a thorough discussion on them have already been published (Andreani, La Franca, & Cristiani, 1993).

3. DATA REDUCTION

Before we averaged all the data belonging to different integrations of the same sky position, low-quality data were rejected.

(1) When the water vapor value was too high, typically greater than 3 mm pww (precipitable water vapor), or

(2) When a spike, due to the abrupt variation of either instrumental or atmospheric behavior, occurred. In practice, this results in a very large standard deviation of the corrupted datum with respect to the mean standard deviation of the entire scan.

The measured values, ΔI_k, are Gaussian distributed with a width equal to the receiver noise in best atmospheric conditions and slightly larger in merely good weather conditions. However, in order to get rid of individual data inconsistent with the underlying Gaussian distribution, data have been reduced as follows (see also Readhead et al. 1989). Within each 200 s scan, 10 s integrations with statistical errors, σ_i, greater than 3 times the rms average of all σ_i, $[(1/N)\sum \sigma_i^2]^{1/2}$, have been rejected. This criterion eliminates spikes due to equipment malfunction or sudden atmospheric variations.

Then, for a given 200 s scan over a sky position (P) we have $\Delta I_k \pm \sigma_k$, where

$$\Delta I_k = \frac{\sum_i (\Delta I_i)/\sigma_i^2}{\sum_i \sigma_i^{-2}}, \tag{2a}$$

$$\sigma_k^2 = \frac{\sum_i (\Delta I_i - \Delta I_k)^2 \sigma_i^{-2}}{(\sum_i \sigma_i^{-2})(M-1)}, \tag{2b}$$

averaged over the 200 s scan ($M = 20$). Therefore, the weighted mean over the N scans (at sky position P) is

$$\Delta I_P = \frac{\sum_{k=1}^{N} \Delta I_k \sigma_k^{-2}}{\sum_{k=1}^{N} \sigma_k^{-2}}, \tag{3a}$$

with a scatter about the mean of

$$\sigma_P^2 = \frac{\sum_{k=1}^{N} (\Delta I_k - \Delta I_P)^2 \sigma_k^{-2}}{\sum_{k=1}^{N} \sigma_k^{-2}}. \tag{3b}$$

For each ΔI_k, a weight is assigned: $w_k = (\sigma_k^2 + \sigma_P^2)^{-1}$, where σ_k^2 represents the variance due to short-term fluctuations, and σ_P^2 that due to medium-term variations. The final *weighted* mean, over the sky position P, is given by

$$\langle \Delta I \rangle_f = \frac{\sum_{k=1}^{N} \Delta I_k w_k}{\sum_{k=1}^{N} w_k}, \tag{4a}$$

with estimated variance

$$\sigma_f^2 = \frac{\sum_{k=1}^{N} (\Delta I_k - \langle \Delta I \rangle_f)^2 w_k}{(N-1)\sum_{k=1}^{N} w_k}. \tag{4b}$$

Rejection of data corresponding to detections is discussed below. Figure 1 reports the histogram of the raw data, which is clearly in agreement with a Gaussian distribution.

3.1. *Test of Systematic Effects*

We have checked whether systematic errors due to long-term atmospheric/instrumental fluctuations affect the data. A

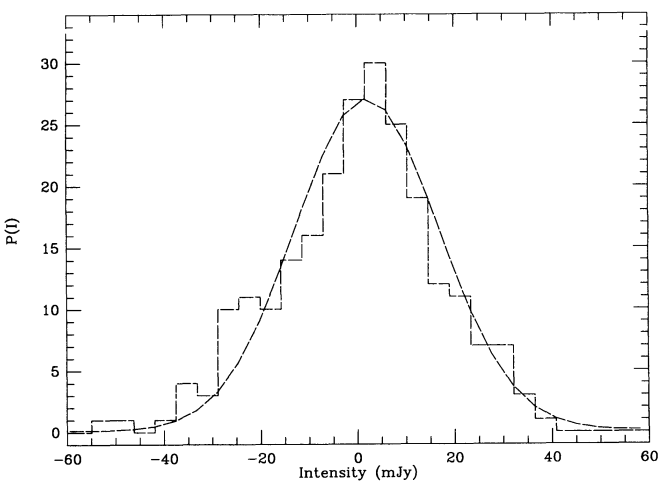

FIG. 1.—Histogram of the SEST raw data for one set of measurements

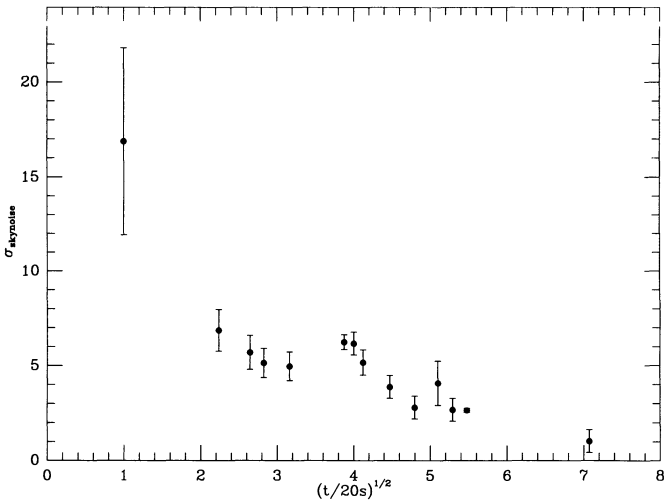

FIG. 2.—Computed standard deviation against the square root of the integration time. The linear decrease with $t^{-1/2}$ is expected for a stationary process affecting the statistical errors. Correlation among errors can be neglected.

plot of the computed variance against the integration time shows a linear decrease of variance with time, as expected for a stationary process affecting the statistical errors (see Fig. 2). This means that, at least for time delays shorter than our maximum integration time, there are no systematic trends. This is due to the high stability both of the receiver and of the good atmospheric conditions during the observations, which have been carried out at night.

4. STATISTICAL ANALYSIS

The problem of inferring upper limits on the sky fluctuations from the measured values has been widely discussed in the literature (see, e.g., Boynton & Partridge 1973; Lasenby & Davies 1983, hereafter LD; Readhead et al. 1989). In the following, we briefly explain the different procedures applied to our data. Both *estimation* theory and *test* theory have been used to derive limits on θ_{sky}, the variance of the distribution of the intrinsic sky fluctuations. The tests have been performed for the three different sets of data at beam separations of 30″ (beam of 11″), 70″ (beam of 24″), and 140″ (beam of 24″). Among the data belonging to the two former samples, there are observations with a signal-to-noise ratio (S/N) greater than 3, which can be due, very likely, to the emission of the source itself. Therefore, in the following we consider two data sets for sky fluctuations in a beam $\phi_b = 11''$ and a beam separation $\phi_s = 30''$ and those in a beam $\phi_b = 24''$ and a beam separation $\phi_s = 70''$: sample A contains all the data except those related to detected objects having a 1.25 mm flux in agreement with an extrapolation of their radio spectrum; sample B contains all observations with S/N < 3.

4.1. *Limits at $\phi_s = 70''$ for $\phi_b = 24''$*

The final weighted averages of the data (eq. [4a]) with 2 σ errors bars (eq. [4b]) as a function of the sky position are shown in Figure 3*a*. Data with S/N > 3 are not reported in this figure. As explained above, we perform the statistical analysis for the two data sets A and B. The statistical tests used involve the computation of (1) the likelihood function and (2) the likelihood ratio.

1. First, we consider, as the most general estimation of the sky fluctuations, the *likelihood* method, which consists of maximizing the joint probability density for the N_f measurements, $\langle \Delta I \rangle_f + \sigma_f$ (eqs. [4a] and [4b]). For uncorrelated fields, the likelihood function reads:

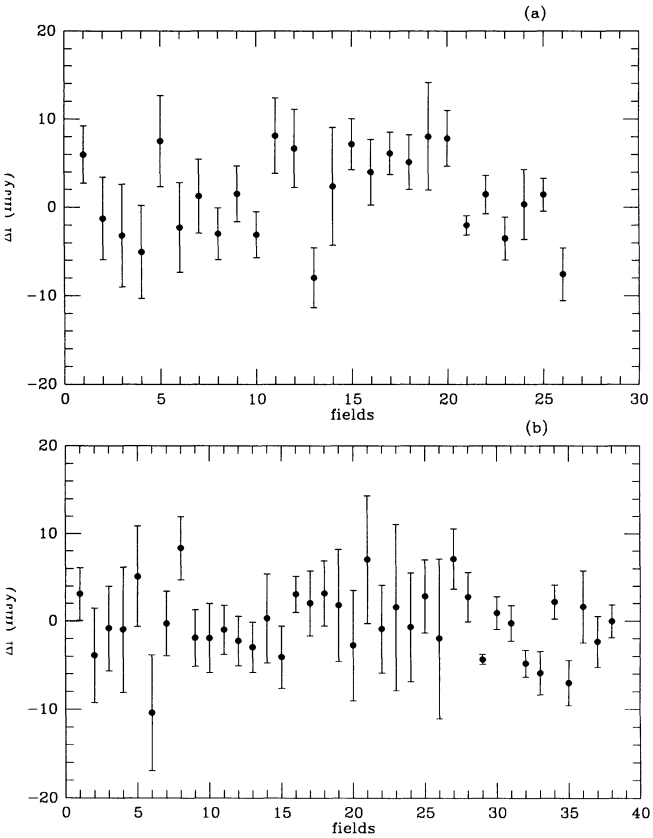

FIG. 3.—(*a*) 70″ data, $\langle \Delta I \rangle_f \pm \sigma_f$ (from eqs. [4a] and [4b]) as a function of the sky position. (*b*) Same as (*a*) for the 140″ data.

$$L(\theta_{\text{sky}}) \equiv \prod_{f=1}^{N_f} [2\pi(\sigma_f^2 + \theta_{\text{sky}}^2)]^{-1/2} \exp\left[\frac{-\langle \Delta I \rangle_f}{2(\sigma_f^2 + \theta_{\text{sky}}^2)}\right]. \quad (5)$$

This function normalized to its maximum value is shown in Figure 4*a* as a solid line (case A). The dashed line corresponds to the likelihood function of the subsample without the *likely* detections (case B).

The value of θ_{sky} for which the likelihood function has its maximum is $\theta_{\text{sky}} = 3.3$ mJy (case A) and 2.9 mJy (case B). Because of the peaks in the likelihood functions, these could be interpreted as detections. To estimate a 95% confidence interval for these values, we consider the value of θ_{sky} for which the likelihood function has fallen to 0.05 of its maximum value. Finally, we find confidence intervals $3.3^{+2.1}_{-1.4}$ and $2.9^{+2.3}_{-1.7}$ for cases A and B, respectively. Bayes's method (see, e.g., Kendall & Stuart 1979) applied to the likelihood function (eq. [5]) with a simple uniform prior distribution, $p(\theta_{\text{sky}})$, gives in this case that $\theta_{\text{sky}} < 4.8$ mJy at 95% and 6.2 mJy at 99.87% (case A) and that $\theta_{\text{sky}} < 4.5$ mJy at 95% and 5.6 mJy at 99.87% (case B). These values are summarized in Table 1.

2. Within the framework of test theory the *likelihood ratio* provides a reliable method to test a hypothesis H against an alternative one, H′, and it has frequently been employed in the past to infer upper limits on sky fluctuations (see, e.g., Boynton & Partridge 1973; LD; Uson & Wilkinson 1984; Readhead et al. 1989). This test provides a critical region between two alter-

TABLE 1

UPPER (AND LOWER) LIMITS ON SKY FLUCTUATIONS AT 30″, 70″, AND 140″ AT 95% CONFIDENCE LEVEL DERIVED WITH DIFFERENT STATISTICAL PROCEDURES

	$\phi_b = 11''$ and $\phi_s = 30''$		$\phi_b = 24''$ and $\phi_s = 70''$		$\phi_b = 24''$ and $\phi_s = 140''$
SAMPLE	Sample B	Sample A	Sample B	Sample A	Sample A
Likelihood (mJy)	<0.73	$0.9^{+0.7}_{-0.4}$	$2.9^{+2.3}_{-1.7}$	$3.3^{+2.1}_{-1.4}$	$2.5^{+1.8}_{-1.1}$
Bayesian (mJy)	<0.57	<1.4	<4.5	<4.8	<3.7
Likelihood ratio (mJy)	<0.57	<1.4	<4.0	<4.3	<3.4
$\Delta T/T$ (final) (10^{-4})	<1.4	<2.4	<2.4	<2.6	<1.9

native hypotheses, i.e., H: $\theta_{\rm sky} = \theta_0$ and H′: $\theta_{\rm sky} = \theta_1$. In particular, if

$$\lambda \equiv \frac{\text{pdf (H)}}{\text{pdf (H')}} \leq k ,$$

H is rejected, while if $\lambda > k$, H is accepted. pdf (H) and pdf (H′) are the probability distributions of the sample under the two alternatives, and the critical region is related to the level of significance or *size* of the test, α, where pdf $(\lambda \leq k \,|\, \text{H}) = \alpha$; i.e., the size α is the probability of rejecting H if H is true. This test is also able to provide a *power* of the test, β; i.e., the power β is the probability of rejecting H if H′ is true (i.e., $1 - \beta$ is the probability of accepting H if H′ is true).

To this end, we have used the estimators given by LD. We wish to test the hypothesis H: $\theta^2_{\rm sky} = 0$ against H′: $\theta^2_{\rm sky} > 0$. This test is given by $\hat{\theta}^2_{\rm sky} > c$, where

$$\hat{\theta}^2_{\rm sky} = \frac{\sum_f (\langle \Delta I \rangle_f - \langle \Delta I \rangle)^2 w_f - (N_f - 1)}{\sum_f w_f [1 - \sum_f w_f^2 / (\sum_f w_f)^2]} ,$$

$$c = \frac{\chi^2_{N_f - 1;\, 1-\alpha} - (N_f - 1)}{\sum_f w_f [1 - \sum_f w_f^2 / (\sum_f w_f)^2]} ,$$

where $w_f = 1/\sigma_f^2$ (eq. [4b]), $\chi^2_{N_f - 1;\, 1-\alpha}$ denotes the $1 - \alpha$ percentage value of χ^2 distribution with $N_f - 1$ degrees of freedom, and $\hat{\theta}^2_{\rm sky}$ is an unbiased estimator of the sky variance, which in this case turns out to be 9.1 mJy^2 and 7.7 mJy^2 for cases A and B, respectively. The statistical quantity c is 2.4 mJy^2 (case A) and 2.9 mJy^2 (case B). It can be shown that the use of $w_f = 1/\sigma_f^2$ instead of $w_f = 1/(\sigma_f^2 + \theta^2_{\rm sky})$ can lead to an overestimation of the final variance (see LD). However, the effect is small, amounting to maximum increases in variance of 9%, 6%, and 2% for the 70″, 140″, and 30″ data, respectively (see below).

The value of $\hat{\theta}^2_{\rm sky}$ for the data shown in Figure 3*a* is significant in rejecting the null hypothesis ($\theta^2_{\rm sky} = 0$), indicating that sky (atmospheric + astronomical) fluctuations are present in our data. However, since these data have been taken toward astronomical sources, these fluctuations could be due to source emission which mimics cosmic background angular variations. In order to evaluate appropriate upper limits to the sky anisotropies, we estimate, as suggested by LD, the following quantity:

$$s^2 = \frac{N_f}{\sum_f w_f} \left\{ \frac{\sum_f w_f [1 - \sum_f w_f^2 / (\sum_f w_f)^2] \theta^2_{\rm sky} + (N_f - 1)}{\chi^2_{N_f - 1;\, 0.05}} \right\}$$

and take as a conservative upper limit at the 95% confidence level the larger of c and s^2. In this case, $s^2 = 17.3$ mJy^2 (case A) and 16.2 mJy^2 (case B). The power of this test is not very high: $\beta = 0.51$.

Table 1 reports the upper limits inferred from the different statistical procedures described above for the two samples A and B. The small discrepancy between the Bayesian value and that found with the likelihood ratio test can be due to a slight overestimation of the measurement errors. It can be shown that an overestimate of the errors causes the limit given by the likelihood ratio test to decrease, while causing that found with the Bayesian method to be enhanced (see Readhead et al. 1989, and references therein, for extensive discussions on this problem). This is stated by the power of the likelihood test. We prefer, therefore, to take as conservative upper limits 4.5 mJy (case B) and 4.8 mJy (case A), i.e., those given by the Bayesian method, aware that these limits can be overestimated.

4.2. *Limits at $\phi_s = 140''$ for $\phi_s = 24''$*

The analysis described above can be extended to larger angular scales by appropriately combining the 70″ data points. In order to get rid of a possible contribution by the target source to the sky fluctuations, we have reduced the data so as to cancel out the signal on the source position. Instead of subtracting each pair of ON-OFF measurements to find the ON-ON value expressed by equation (1), we have added them. This means that the resulting datum will be

$$\Delta I = I_A - I_B , \qquad (6)$$

where A and B are sky positions beside the source at a relative distance of twice the chop throw—i.e., for the SEST observations; 140″. It must be noted that in this case we lose 15%–20% sensitivity to detect sky fluctuations with respect to triple-beam data.

The resulting measurements have been reduced as described in § 3, and Figure 3*b* reports the final weighted averages. The statistical analysis described in § 4.1 gives the following results. The likelihood function is plotted in Figure 4*b* and has its maximum value at $\theta_{\rm sky} = 2.5$ mJy, with a 95% confidence range of 1.4–4.3 mJy. Again this value can be considered as a detection. This means that fluctuations are still present in the data although the subtraction of data as in equation (6) should have been sufficient to get rid of the source emission. The 95% and 99.87% upper limits given by Bayes's formula are 3.7 and 5.1, respectively, while that at 95% given by the likelihood ratio test is 3.4 mJy (the power of this latter is $\beta = 0.81$). This test states that $\theta^2_{\rm sky} > c$; i.e., we cannot reject the null hypothesis $\theta^2_{\rm sky} = 0$ at the 95% confidence level. The detected fluctuations can be ascribed either to higher order terms of the atmospheric emission and/or to astronomical sources as discussed in § 5. All the upper limits found with the three different methods are summarized in Table 1.

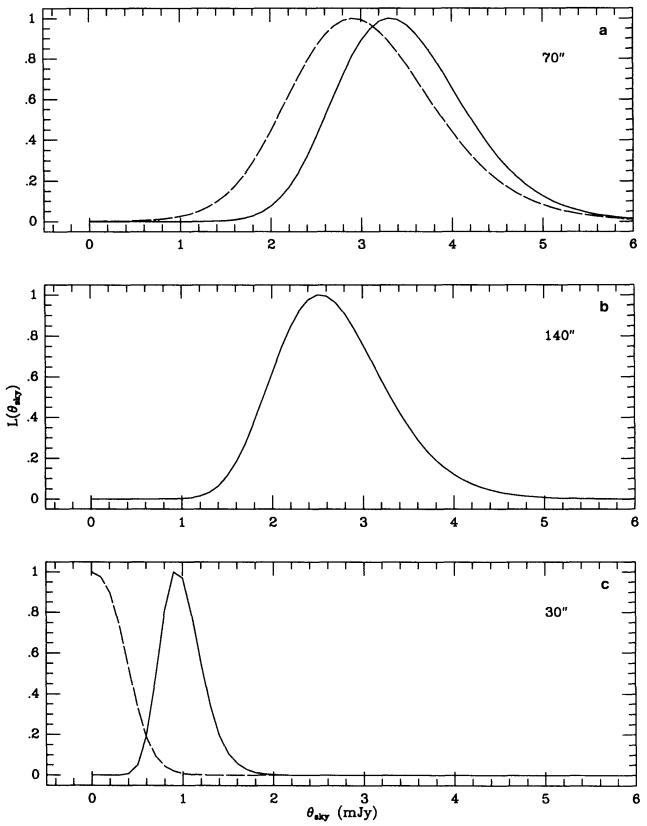

FIG. 4.—Maximum likelihood functions for the three sets of data considered in this work. (*a*) 70″ data: all data (*solid line*) and data without "detections" (*dashed line*); (*b*) 140″ data; and (*c*) 30″ data: all data (*solid line*) and data without "detections" (*dashed line*).

4.3. *Limits at $\phi_s = 30''$ for $\phi_b = 11''$*

IRAM data have been reduced as described in § 3. In order to increase the statistical significance of the test, we have added to our measurements those taken by Kreysa & Chini (1988) with the same instrumentation. We have discarded from Kreysa & Chini's data on 25 quasars the three objects (2041−109, 2130+099, and 1353+186) having a 1.25 mm flux consistent with an extrapolation of the radio spectrum and have kept the two objects that, although detected at 6 cm with the VLA[2] (Kellerman et al. 1989), have a 1.25 mm flux not matching the radio spectrum. Our procedure appears to be different from that applied by Kreysa & Chini, who kept 21 objects, discarding the two objects having a radio-quiet–type spectrum and keeping 2130+099 whose 1.25 mm flux appears to be in agreement with an extrapolation of its radio spectrum. A similarly analysis on 21 objects from the Kreysa & Chini sample has been also performed by BCH91 and Church et al. (1993). However, these authors do not specify which objects have been discarded from the sample.

The following analysis consider the two 30″ data sets—sample A, radio-quiet–type sources, and sample B, only nondetections (see above in the introduction of § 4 for details). Figure 4*c* shows the maximum likelihood functions for the two samples. In case A, this function clearly shows a detection at $\theta_{sky} = 0.9$ mJy, while in case B, the maximum likelihood function has its maximum value at $\theta_{sky} = 0$ and falls to 5% of its peak value at $\theta_{sky} = 0.73$ mJy. The Bayesian method gives an upper limit of 1.4 mJy at 95% for case A, and 0.57 mJy at 95% for case B. For case A, the $\hat{\theta}^2_{sky}$ of the likelihood ratio test is 0.8 and the upper limit at the 95% confidence level is given by the statistical quantity $s^2 = 1.9$ mJy^2, i.e., 1.4 mJy. For case B, the likelihood ratio test chooses the statistical quantity $c = 0.57$ mJy at the 95% confidence level. In this case, in fact, $\hat{\theta}^2_{sky} < c$, and no sky fluctuations can be inferred from these data. The latter value is the one we quoted as a conservative upper limit for the sky fluctuations.

[2] The VLA is a facility of the National Radio Astronomy Observatory, which is operated by Associated Universities, Inc., under contract with the National Science Foundation.

4.4. *Conversion to $\Delta T/T$*

We have converted the above upper limits to temperature fluctuations of the microwave sky by means of: $\Delta T/T = \Delta I/I \int_{x_1}^{x_2} (e^x - 1/xe^x)dx$, where the integral is performed over the filter bandwidth and the sky intensity is calculated by integrating over the filter bandwidth and the solid angle covered by the beam, supposed to be Gaussian ($\Omega_{beam} = (\pi/\ln 2)(\theta_{FWHM}/2)^2$. Note that three-beams data test the statistical sky fluctuations with an efficiency of $3/2^{1/2}$, with respect to double-beam measurements.

4.5. *Comparison with Other Results at Similar Frequencies*

Kreysa & Chini (1988) have already given an upper limit of the sky fluctuations at 30″ of 2.6×10^{-4}. Their data have been reanalyzed by BCH91 with the same methods used in this work, and the upper limit found with the Bayesian analysis is 3.2×10^{-4}. Note that a precise comparison between our analysis and their cannot be made because of the different data sets used in the statistical analyses.

Church et al. (1993) report a value of 1.4×10^{-3} (Bayesian estimate) for the upper limit for the sky fluctuations at 800 μm. Despite the poorer sensitivity, their limit gives competitive constraints to dust models although not as stringent as those at 1300 μm, as discussed by Church et al. and in BCH91.

4.6. *Limits on the Autocorrelation Function*

Figure 5 shows the convolution of the sky autocorrelation function, $CF(\phi) = \langle I(x_1)I(x_2)\rangle$, with the antenna beam pattern approximated by a Gaussian, $(1/4\pi\phi_0)\exp(-\phi^2/4\phi_0^2)$, where $\phi_0 = 0.425\phi_{FWHM}$. For a three-beam experiment, this convolution becomes (see Readhead et al. 1989)

$$\langle \Delta I^2 \rangle = \tfrac{3}{2}CF(\phi_0, 0) - 2CF(\phi_0, \phi_s) + \tfrac{1}{2}CF(\phi_0, 2\phi_s) ,$$

while for a double-beam experiment, it reads

$$\langle \Delta I^2 \rangle = CF(\phi_0, 0) - CF(\phi_0, \phi_s) ,$$

ϕ_s being the beam separation. The results shown in Figure 5 have been performed assuming that the sky autocorrelation function is Gaussian with coherence angle ϕ_c and using the Bayesian upper limits listed in Table 1. As expected all three experimental setups show reduced sensitivity for coherence angles smaller than the beam size because of averaging over many independent fluctuations.

5. DISCUSSION

We briefly discuss the results of this work in terms of (1) dust models computed by BCH91 and (2) the galaxy contribution predicted by Franceschini et al. (1989, 1991).

1. The quoted upper limits (Table 1) can be compared with

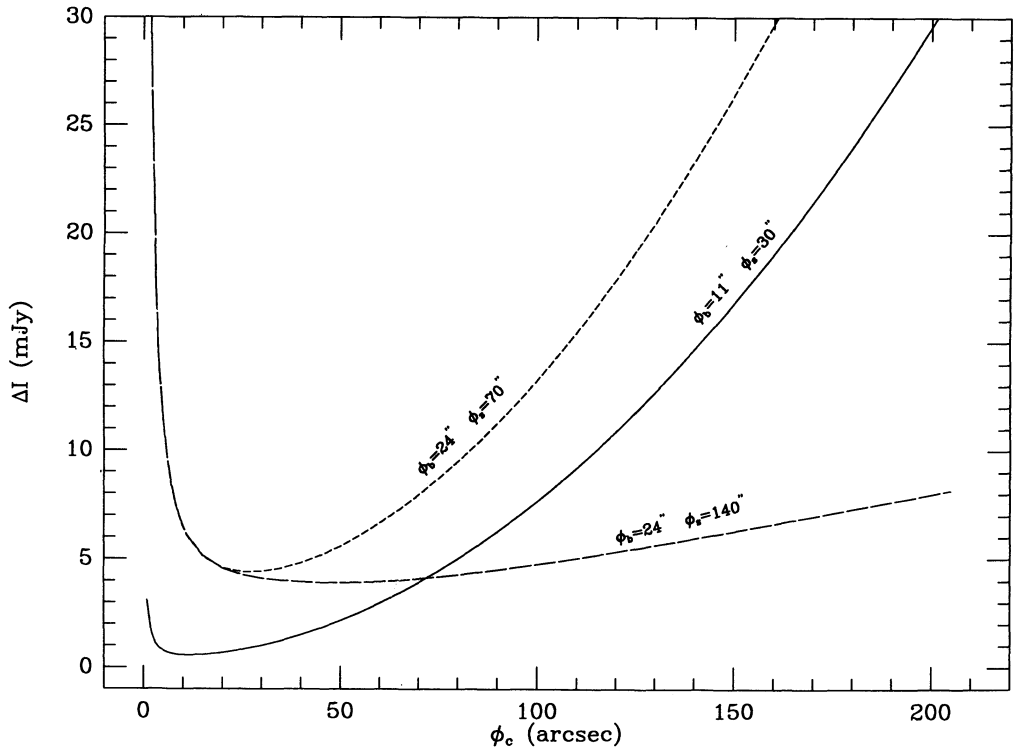

FIG. 5.—Limits on sky fluctuations, ΔI, for a Gaussian autocorrelation function with coherence angle, ϕ_c. Sample B data are used (see text for details). The beam pattern is modeled as a Gaussian.

the predictions of dust models by BCH91. Anisotropies in these models arise both from Poissonian fluctuations in the number of the emitting sources ($\Delta T/T \propto n_G^{-1/2}$, where n_G is the comoving number density of galaxies) and from source clustering if the emitting sources cluster as normal galaxies do. Indeed, a detailed comparison with these models can be made only for IRAM data, since BCH91 convolved the predicted correlation function of the radiation pattern with a filter function related to that experiment. IRAM data exclude most of the $\Delta T/T$ predicted in case of a Poissonian distribution of sources, except for those predicted by models 8, 12, and 13. Our limit ($\Delta T/T < 1.4 \times 10^{-4}$), together with the predictions of model 12, requires a source density of $n_G > 0.015$ and a correlation length at the emission redshift $r_0(z_e) < 10.4$. Mpc. If fluctuations due to source clustering are added to the Poissonian ones, the basic results do not change.

To compare our limits at larger angular scales with the model predictions, we scale the predicted $\Delta T/T$ by a factor proportional to $\theta_{\rm FWHM}^{-1}$ for the Poisson distribution of the emitting sources and to $\theta_{\rm FWHM}^{-0.4}$ for clustered sources. Furthermore, the predicted $\Delta T/T$ for double-beam data have been enhanced by a factor of 15%–20%. Only models 2, 4, 8, 12, 13, and 14 (contribution of source clustering added to the Poissonian one) are not ruled out by the observed upper limits. For instance, for model 2, SEST data constrain the lower bound on the galaxy abundance at $n_G > 0.022$ and the upper bound on the correlation length at the emission redshift $r_0(z_e) < 6.3$ Mpc.

2. Franceschini et al. (1989, 1991) predict a confusion limit at 1.3 mm of $\Delta T/T \sim 2$–5×10^{-5} in a beam of 24″. Even if we allow the predicted value to increase because of enhanced cell-to-cell fluctuations due to galaxy clustering, it would be hard to ascribe the detected fluctuations to the confusion limit of a population of unresolved evolving sources. Detailed calculations taking into account the experimental setup must be performed before any meaningful comparison with these data can be carried out. If we take their predicted value without any correction, their limits are at least 3 times smaller than the experimental upper limits reported in Table 1.

Finally, it must also be mentioned that clusters of galaxies along the line-of-sight can significantly contribute to sky fluctuations via the Sunyaev-Zeldovich effect on the CBR. There are no detailed calculations at high frequencies; however, it is very likely that the predicted values still lie below the current upper limits at millimetric wavelengths (e.g., Markevitch et al. 1992). As already stated in § 4, it is very likely that at least part of the detected sky fluctuations are due to the atmosphere. Future experiments must address the problem that, unless the atmospheric contribution can be quantified, these fluctuations can prevent any detection at millimetric wavelengths. The atmospheric contribution can be quantified by monitoring the atmospheric emission fluctuations by means of a multiple channel photometer (see, e.g., Andreani et al. 1991).

I have benefited from useful conversations with A. Franceschini, who helped to improve this paper substantially. I thank L. Toffolatti and S. Cristiani for helpful discussions.

REFERENCES

Andreani, P., Dall'Oglio, G., Martinis, L., Piccirillo, L., Pizzo, L., Rossi, L., & Venturino, C. 1991, A&A, 249, 299
Andreani, P., La Franca, F., & Cristiani, S. 1993, MNRAS, 261, L35
Bond, J. R., Carr, B. J., & Hogan, C. J. 1986, ApJ, 306, 428
———. 1991, ApJ, 367, 420 (BCH91)
Boynton, P. E., & Partridge, R. B. 1973, ApJ, 181, 243
Church, S. E., Lasenby, A. N., & Hills, R. E. 1993, MNRAS, 261, 705
Franceschini, A., Toffolatti, L., Danese, L., & De Zotti, G. 1989, ApJ, 334, 35
Franceschini, A., Toffolatti, L., Mazzei, P., Danese, L., & De Zotti, G. 1991, A&AS, 89, 285
Gautier, T. N., Boulanger, F., Pérault, M., & Puget, J. L. 1992, AJ, 103, 1313
Kellermann, K. L., Sramek, R., Schmidt, M., Shaffer, D. B., & Green, B. 1989, AJ, 98, 1195
Kendall, M., & Stuart, A. 1979, The Advanced Theory of Statistics (London: Griffin)
Kreysa, E. 1990, in From Ground-Based to Space-Born Sub-mm Astronomy, ed. J.-P. Swings & D. Fraipont (ESA SP-314) (Noordwijk: ESA Publications Division), 265
Kreysa, E., & Chini, R. 1988, in Proc. 3d ESO/CERN Symp. on Astronomy, Cosmology and Fundamental Physics, ed. M. Caffo, R. Fanti, G. Giacomelli, & A. Renzini (Dordrecht: Kluwer), 433
Lasenby, A. N., & Davies, R. D. 1983, MNRAS, 203, 1137 (LD)
Liebe, H. J. 1983, NTIA Report 83-187
Markevitch, M., Blumenthal, G. R., Forman, W., Jones, C., & Sunyaev, R. A. 1992, ApJ, 395, 326
Negroponte, J. 1986, MNRAS, 222, 19
Oliver, S. J., Rowan-Robinson, M., & Saunders, W. 1992, MNRAS, 256, 15p
Partridge, R. B., & Peebles, P. J. 1967, ApJ, 148, 377
Readhead, A. C. S., Lawrence, C. R., Myers, S. T., Sargent, W. L. W., Hardebeck, H. E., & Moffet, A. T. 1989, ApJ, 346, 566
Rowan-Robinson, M., Negoponte, J., & Silk, J. 1979, Nature, 281, 635
Saunders, W., Lawrence, A., Efstathiou, G., Kaiser, N., Ellis, R. S., & Frenk, C. S. 1990, MNRAS, 242, 318
Stecker, F. W., Puget, J. L., & Fazio, G. G. 1977, ApJ, 214, L51
Tinsley, B. 1973, A&A, 24, 89
Uson, J. M., & Wilkinson, D. 1984, ApJ, 235, 681
Wright, E. L., et al. 1993, *COBE* preprint